Compressive sensing spectrometry based on liquid crystal devices

Yitzhak August and Adrian Stern*

Department of Electro Optical Engineering, Ben-Gurion University of the Negev, Israel
**Corresponding author: stern@bgu.ac.il*

Received July 23, 2013; revised October 9, 2013; accepted October 28, 2013;
posted October 28, 2013 (Doc. ID 194484); published November 21, 2013

We present a new type of compressive spectroscopy technique employing a liquid crystal (LC) phase retarder. A tunable LC cell is used in a manner compliant with the compressive sensing (CS) framework to significantly reduce the spectral scanning effort. The presented optical spectrometer consists of a single LC phase retarder combined with a single photo detector, where the LC phase retarder is used to modulate the input spectrum and the photodiode is used to measure the transmitted spectral signal. Sequences of measurements are taken, where each measurement is done with a different state of the retarder. Then, the set of photodiode measurements is used as input data to a CS solver algorithm. We demonstrate numerally compressive spectral sensing with approximately ten times fewer measurements than with an equivalent conventional spectrometer.

OCIS codes: (170.0170) Medical optics and biotechnology; (280.0280) Remote sensing and sensors; (300.0300) Spectroscopy; (310.0310) Thin films; (110.1758) Computational imaging; (110.4234) Multispectral and hyperspectral imaging.
http://dx.doi.org/10.1364/OL.38.004996

Spectroscopic analysis plays an increasingly important role in the fields of biology and medicine [1], hyperspectral imaging [2–4] and many more. As a result of the growing use of spectrometric systems within different optical systems, there is a continuously increasing need to design spectroscopic systems with improved performance in terms of spectral acquisition time, resolution, spectral range, signal-to-noise ratio (SNR), sensitivity, and system size.

Most conventional spectrometers are based on spectral component separation; the different spectral components of light that pass through the separation device are measured by an irradiance sensor; thus, providing information about the spectral power distribution. This is commonly achieved with various devices, such as colored and tunable filters, with which the different wavelengths are measured at different times, or by employing dispersive prisms or diffractive gratings, with which different wavelengths are measured at different angles or locations. This ability to select spectral components of light is the central part of common spectroscopy. The separation of light allows us to determine what energies of light are absorbed or emitted by a particular sample.

In this Letter, we describe a method using a single tunable phase retarder, together with a single photo sensor (e.g., photo diode), to implement compressive sensing (CS) spectral measurements. A nematic liquid crystal (LC) cell can be implemented as a tunable birefringent material to obtain spectral dependence transmission. As opposed to classic methods of spectral acquisition, where a narrow band spectral filter (band pass filter) is desired to select narrow band spectral components, with the proposed method the LC is set to modulate the spectrum over a wide spectral band in a manner that is compliant with CS theory [5–9].

"Compressive sensing," a.k.a. "compressed sensing" (CS) [5–9] is a framework for the acquisition of signals from significantly fewer measurements than are needed according to the traditional Shannon–Nyquist sampling theory. In the following, we shall provide a brief introduction to CS in the context of the proposed method. Let the vector $\mathbf{f} \in \mathbb{R}^{N\times 1}$ represent a physical signal, which, in our case, presents a set of N spectral bands of the optical signal. According to the CS paradigm, the N spectral bands can be recovered from only $M < N$ multiplexed measurements $\mathbf{g} \in \mathbb{R}^{M\times 1}$. The process of spectral measurement can be described by a linear vector matrix equation $\mathbf{g} = \mathbf{\Phi f}$, where $\mathbf{\Phi} \in \mathbb{R}^{M\times N}$ represents the sensing matrix. In this form, the i^{th} element of $\mathbf{g}$ represents a projection between the vector $\mathbf{f}$ and i row of the matrix $\mathbf{\Phi}$:

$$g_i = [\phi_i(\lambda_1)\ldots\phi_i(\lambda_k)\ldots\phi_i(\lambda_N)] \cdot \begin{bmatrix} f(\lambda_1) \\ \vdots \\ f(\lambda_k) \\ \vdots \\ f(\lambda_N) \end{bmatrix}, \qquad (1)$$

that is, the set of spectral measurements g_i, $i = 1, 2, \ldots, M$ is the result of projection of the input spectral information over different modulating functions ϕ_i. In physical systems, the structure of $\mathbf{\Phi}$ depends on the design of the optical device and the system. By changing some physical parameters (e.g., voltage across the LC retarder), various modulations can be obtained.

Compressive sensing relies on the assumption that the signal has some sparse or compressible representation in some domain [5–9]. In vector matrix formalism, the vector $\mathbf{f}$ can be represented in the form of $\mathbf{f} = \mathbf{\Psi\alpha}$, where $\boldsymbol{\alpha}$ is a vector of components in the domain of $\mathbf{\Psi}$. For most physical signals, it is possible to find an appropriate,$\mathbf{\Psi}$ such that the decomposition coefficients vector $\boldsymbol{\alpha}$ is sparse; that is, the vector $\boldsymbol{\alpha}$ contains mainly zeros or near-zero value elements. We denote the number of nonzero elements in $\boldsymbol{\alpha}$ by k. CS theory applies in the case where the relation between the numbers of spectral bands,N, to the number of multiplexed spectral

measurements, M, and the number of nonzero elements, k, obeys the relation $k < M \ll N$.

In the final step of the CS process, the N spectral bands of $\mathbf{f}$ are reconstructed from the set of M multiplexed measurements, $\mathbf{g}$. This stage can be accomplished by using an ℓ_1-type minimization algorithm [10,11] or other. A common practical approach is by calculating the signal $\hat{\mathbf{f}}$ from the estimated coefficients $\hat{\boldsymbol{\alpha}}$:

$$\hat{\mathbf{f}} = \boldsymbol{\Psi}\hat{\boldsymbol{\alpha}}; \qquad \hat{\boldsymbol{\alpha}} = \min_{\boldsymbol{\alpha}}\{\|\mathbf{g} - \boldsymbol{\Phi}\boldsymbol{\Psi}\boldsymbol{\alpha}\|_2^2 + \gamma\|\boldsymbol{\alpha}\|_1\}, \quad (2)$$

where $\|\cdot\|_1$ denotes the ℓ_1 norm and the coefficient γ is a regularization parameter. Another way to estimate $\hat{\mathbf{f}}$ is by using the total variation (TV) norm as a penalty function, as an alternative to the ℓ_1 norm.

In recent years, several methods have been presented that apply CS for spectroscopic imaging [12–15] and for polarimetric imaging spectrometry [16]. Generally, CS spectrometry methods implement the system model $\mathbf{g} = \boldsymbol{\Phi}\mathbf{f}$ by capturing a multiplexed set of measurements; each single measurement at the photo sensor is a result of a combination of many spectral components with different known weights. In this kind of system, a diffractive or dispersive element is used to split the spectral information into different angles in space. The spectral information is then coded using a spatial mask that is implemented by a coded aperture or a digital micro mirror device (DMD). After the coded aperture encodes the different spectral rays, they are focused using a converging lens and collected by the sensor to provide a single spectral projection [see Eq. (1)]. Multiple measurements are performed, each with a different DMD state or coded aperture pattern. Another method to capture 2D spatial information together with 1D spectral information (hyperspectral imaging) is called coded aperture snapshot spectral imaging (CASSI) [12].

We note that, in the previous spectral CS methods [12–16], the multiplexing is performed in the spatial domain and in a discrete form (due to the pixelated DMD or spatial mask). In contrast, we present here a method that performs spectral multiplexing directly in the spectral domain without the need for spectral-to-spatial conversion.

In general, multiplexing in the spectral domain can be performed by passing the polychromatic light through a periodic structure or through an alternating thin film structure with LC in between to generate a tunable spectral response. Figure 1 describes the measurement principle using such a device. In Fig. 1, the spectral signal, $f(\lambda)$, is modulated by passing it through the tunable optical thin film structure and the modulated (reflected or transmitted) signal is captured by a photo sensor. The i^{th} measurement of g_i is given by

$$g_i = \int f(\lambda) \cdot h_i(\lambda) \mathrm{d}\lambda, \quad (3)$$

where $h_i(\lambda)$ represents the total spectral responses of the entire optical system. It can be written as the product $h_i(\lambda) = \alpha(\lambda) \cdot \phi_i(\lambda)$, where the spectral calibration function $\alpha(\lambda)$ accounts for the spectral responses of all other optical components. For simplicity, in this work we assume $\alpha(\lambda) \approx 1$; i.e., the system response $\alpha(\lambda)$ changes very slowly over the desired spectrum. In cases where $\alpha(\lambda)$ cannot be approximated as such, the reconstructed spectral information needs to be divided by a pre measured $\alpha(\lambda)$.

In this work, we consider the implementation of thin film structures by tunable birefringence phase retardation, such as a nematic LC cell in the typical structure [17] (Fig. 2).

Liquid crystal variable retarders [18] consist of a transparent cell filled with a solution of LC molecules that functions as a variable wave plate. The orientation of the LC molecules is determined by the alignment layer in the absence of an applied voltage. When a low frequency AC voltage is applied, the molecules will change from their default orientation according to the amplitude of the AC voltage or the electric field applied over the molecules. Hence, the phase offset of a linearly polarized beam of light can be actively controlled by varying the applied voltage [19,20].

The electric field applied between the electrodes induces birefringence, Δn_i. The optical retardation is proportional to the induced birefringence, $\Delta n_i = n_{e,i} - n_o$, where n_e is the extraordinary refraction coefficient and n_o is the ordinary refraction coefficient. For a given cell with gap, d, the phase retardation (phase difference) at wavelength, λ, is given by $\delta_i = (2 \cdot \pi \cdot \Delta n_i d)/\lambda$ and, therefore, the intensity of light traversing the cell is $f(\lambda)\phi_i(\lambda)$; the spectral modulation depends on the optical retardation [17] and has the form of:

$$\phi_i(\lambda) = I_i(\lambda)/I_0(\lambda) \propto \sin^2(\delta_i(\lambda)/2). \quad (4)$$

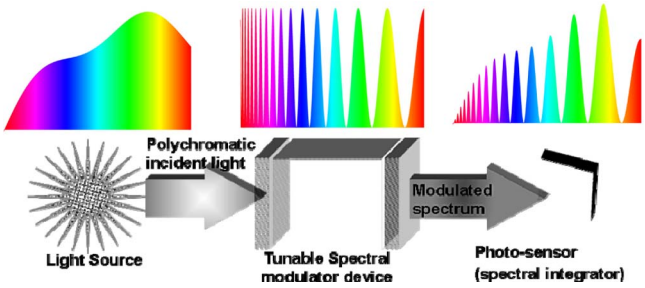

Fig. 1. Figurative description of spectral modulation by passing through the structure of a LC-based retarder.

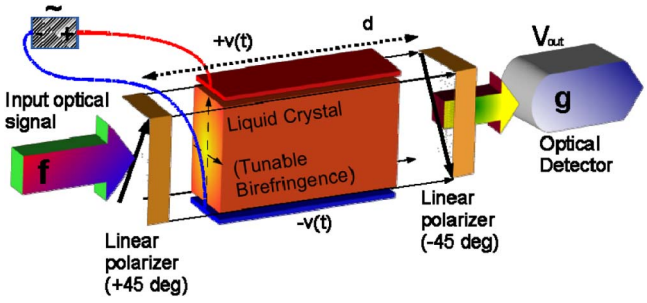

Fig. 2. Liquid crystal variable retarder used as a spectral modulator and a photo sensor that integrates the modulated spectrum. The spectral modulation at the output is a function of the birefringence, which can be controlled by the applied voltage over the cell.

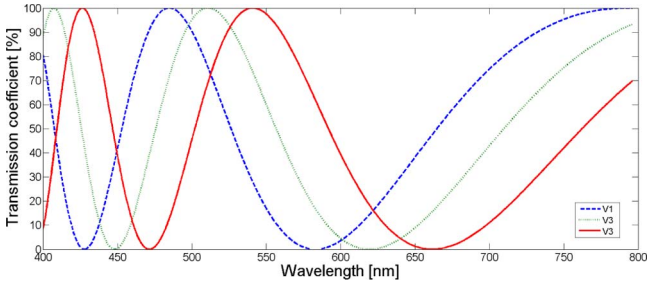

Fig. 3. Three different spectral responses obtained by changing the electrical potential over the LC retarder cell (theoretical model).

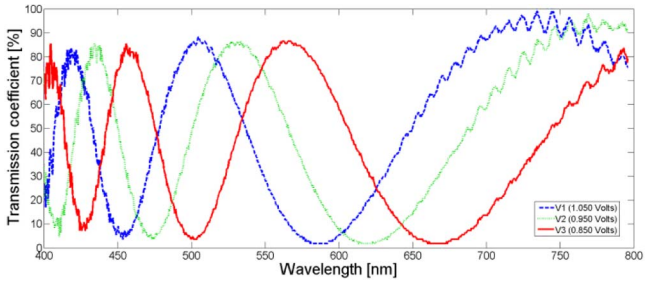

Fig. 4. Example for spectroscopic transmission measurements of three different spectral responses of LC cell. These spectral responses were obtained by changing the electrical potential (1.05, 0.95, and 0.85 V) over the experimental LC retarder cell.

In Eq. (4) $I_i(\lambda)$ denotes the i^{th} modulated signal obtained by tuning the cell to the i^{th} state corresponding to the i^{th} birefringence Δn_i, and $I_0(\lambda)$ is the input spectral information. Figure 3 illustrates typical theoretical spectral responses, $\phi_i(\lambda)$, of an LC variable phase retarder at different Δn_i corresponding to different voltages applied over the cell. It can be seen that the spectral modulations have multiple peaks over a wide spectral range and exhibit low mutual overlapping (i.e., low mutual coherence), which are desired features for CS operators.

Thus, it can be seen that generation of different Δn_i provides a way to modulate the spectral signal with different modulation functions. Using the vector notation previously described, the set of modulated measurements may be written as $\mathbf{g} = \mathbf{\Phi f}$, where, in our case, the sensing operator is

$$\mathbf{\Phi} = \underset{M}{\begin{pmatrix} \sin^2\left(\frac{1}{2}\delta_1(\lambda_1)\right) & \cdots & \sin^2\left(\frac{1}{2}\delta_1(\lambda_N)\right) \\ \vdots & \sin^2\left(\frac{1}{2}\delta_i(\lambda_j)\right) & \vdots \\ \sin^2\left(\frac{1}{2}\delta_M(\lambda_1)\right) & \cdots & \sin^2\left(\frac{1}{2}\delta_M(\lambda_N)\right) \end{pmatrix}}^{N} \tag{5}$$

The sensing matrix in Eq. (5) contains a large number of off-diagonal nonzero entries, which is in great contrast to the common Lyot, or Solc birefringent filter [20–23]. The Lyot filter is a common LC filter device built of multiple retarder stages to obtain a narrow filter with high spectral resolution. As a narrow band filter, $\mathbf{\Phi}$ would have off-diagonal entries close to zero.

The structure of the sensing matrix in Eq. (5) resembles partial Fourier matrices that are common in CS theory [24]. This is better appreciated if elements of $\mathbf{\Phi}$ in Eq. (5) are expressed in terms of frequency rather than wavelength. In such a case, $\phi_i = 1/2 - 1/2\cos(\beta_i\omega)$, where ω is the angular frequency and β_i are parameters depending on factors that, in principle, are randomly chosen.

Figure 4 illustrates spectral distributions obtained in a virtual experiment that simulated the sensing process. In that simulation, we used real spectral responses, $\phi_i(\lambda)$, from an in-house-built LC cell. The cell's spectral responses are measured only once in the calibration step. In this example (Fig. 4), a lab-made LC cell (13 μm at E44 type of nematic LC) was fabricated and its spectral response was measured by a standard spectrometer. Spectral modulations were generated and measured by changing the potential from 0to 10 V, with increments of 0.05–0.5 V.

The spectral resolution of the spectrometer used for the calibration process is 0.4 nm. In the calibration step, 1024 spectral bands in the range of 400.1–796.1 nm were measured to characterize each $\phi_i(\lambda)$. In this way, a set of 108 spectral responses $\{\phi_i(\lambda)\}_{i=1}^{108}$ were obtained and used as the rows of the system matrix $\mathbf{\Phi} \in \mathbb{R}^{108\times1024}$. These sets of LC spectral responses provide the spectral sensing operator $\mathbf{\Phi}$; each element over the rows of $\mathbf{\Phi}$ represents transmission at a different spectral band. A CS LC spectrometer was competently simulated, based on the measured $\mathbf{\Phi}$. The spectral signal shown in Fig. 5 is that of biological soil crusts (biogenic crust-like spectra). Biogenic soil crust consists of a dense growth of many small organisms, like cyanobacteria, mosses, lichens, algae, fungi, and/or bacteria in arid regions worldwide. Those small organisms play an important role in many arid and semi-arid ecosystems. Therefore, mapping the crusts, based on spectral properties, is important [25,26].

Figure 5 compares the spectral signal reconstructed with our method ("reconstructed") to that measured directly with a conventional spectrometer signal ("source"). The number of spectral bands are $N = 1024$. The CS reconstruction was obtained using $M = 108$ spectral sensing vectors; hence, the signal is reconstructed from about 10% of the samples. To solve the ℓ_1-type minimization problem in Eq. (2) we used TwIST solver [10]. As for the sparsifying operator, $\mathbf{\Psi}$, we considered various common

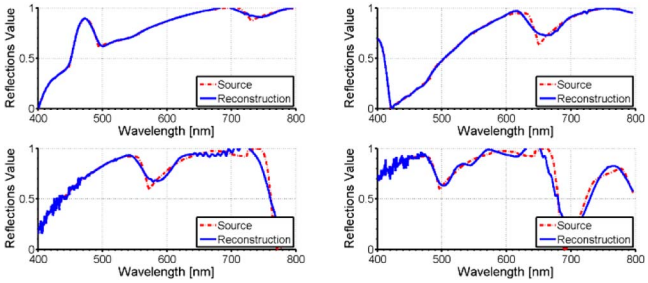

Fig. 5. Directly measured (continuous line) and reconstructed (dashed line) biogenic crust-like spectra. The spectral data has $N = 1024$ samples and the CS spectrum is recovered from $M = 108$ measurements ("coif3" sparsifying operator). Peak SNR values for the reconstructions are 39.6, 33.8, 23.6 and 22.6 dB for spectra A-D, respectively.

wavelet transforms (e.g., Haar, Daubechies 2-4, Symlets 3, Coiflets 3). All these wavelet transforms exhibited good compressibility performance ($k/N \sim 1$–4%). It should be noted that, for specific tasks with a prior knowledge about the expected spectral signal, as often is the case, then a spectral dictionary can be used instead for even better performance (i.e., higher peak SNR values for a given number of CS measurements, or, alternatively, a lower number of measurements for a given peak SNR). The results displayed in Fig. 5 were obtained using the Coiflets 3 wavelet transform as sparsifying operator, which was found to provide the best peak SNR results and lowest coherence to the sensing operator.

In conclusion, a new method of optical compressive spectrometry employing nematic LC phase retardation was presented. The proposed spectrometer consists of only a single nematic LC phase retarder combined with a single photo detector. The spectral power distribution is indirectly measured and reconstructed following a CS approach. The use of an LC retarder with known spectral response (spectrally calibrated cell), in conjunction with CS techniques, provides numerous benefits compared with conventional spectroscopic and spatially based CS methods. Specifically, the proposed method may facilitate: (1) reduction of acquisition time, (2) reduction of the number and the size of detectors, (3) reduction of system size and complexity, (4) reduction of system costs, (5) reduction of noise, and (6) reduction of power loss.

Adrian Stern wishes to thank the Israel Science Foundation (grant no. 1039/09). The authors wish to thank Miri Gelbaor Kirzhner for providing the LC retarder spectroscopic measurements.

References

1. R. Richards-Kortum and E. Sevick-Muraca, Annu. Rev. Phys. Chem. **47**, 555 (1996).
2. M. T. Eismann, *Hyperspectral Remote Sensing* (SPIE, 2012).
3. T. A. Warner, M. D. Nellis, and G. M. Foody, *The Sage Handbook of Remote Sensing* (Sage, 2009).
4. P. S. Thenkabail, J. G. Lyon, and A. Huete, *Hyperspectral Remote Sensing of Vegetation* (CRC Press, 2012).
5. D. L. Donoho, IEEE Trans. Inf. Theory **52**, 1289 (2006).
6. E. J. Candes and M. B. Wakin, IEEE Signal Process. Mag. **25** (2), 21 (2008).
7. Y. C. Eldar and G. Kutyniok, *Compressed Sensing: Theory and Applications* (Cambridge University, 2012).
8. M. Elad, *Sparse and Redundant Representations* (Springer, 2010).
9. R. Baraniuk, IEEE Signal Process. Mag. **24**, 118 (2007).
10. J. M. Bioucas-Dias and M. A. T. Figueiredo, IEEE Trans. Image Process. **16**, 2992 (2007).
11. M. A. T. Figueiredo, R. D. Nowak, and S. J. Wright, IEEE_J. Sel. Topics Signal Process. **1**, 586 (2007).
12. A. Wagadarikar, R. John, R. Willett, and D. Brady, Appl. Opt. **47**, B44 (2008).
13. Y. August, C. Vachman, Y. Rivenson, and A. Stern, Appl. Opt. **52**, D46 (2013).
14. T. Sun and K. Kelly, in *Computational Optical Sensing and Imaging* (Optical Society of America, 2009), pp. TuA5.
15. H. Arguello and G. Arce, in *Imaging Systems Applications* (Optical Society of America, 2011), pp. TuA4.
16. F. Soldevila, E. Irles, V. Durán, P. Clemente, M. Fernández-Alonso, E. Tajahuerce, and J. Lancis, Appl. Phys. B, 1 (2013).
17. A. Yariv and P. Yeh, *Optical Waves in Crystals* (Wiley, 1984).
18. P. Yeh and C. Gu, *Optics of Liquid Crystal Displays* (Wiley, 2009).
19. J. Beeckman, K. Neyts, and P. J. Vanbrabant, Opt. Eng. **50**, 081202 (2011).
20. O. Aharon and I. Abdulhalim, Opt. Express **17**, 11426 (2009).
21. J. W. Evans, J. Opt. Soc. Am. **39**, 229 (1949).
22. J. W. Evans, J. Opt. Soc Am. **48**, 142 (1958).
23. R. Hamdi, R. M. Farha, S. Redadaa, B. Benkelfat, D. Abed, A. Halassi, and Y. Boumakh, ICT Telecommunications, 19th International Conference (2012), pp. 1–4.
24. J. Romberg, SIAM J. Imaging Sci. **2**, 1098 (2009).
25. A. Karnieli, G. J. Kidron, C. Glaesser, and E. Ben-Dor, Remote Sens. Environ. **69**, 67 (1999).
26. B. Weber, C. Olehowski, T. Knerr, J. Hill, K. Deutschewitz, D. C. J. Wessels, B. Eitel, and B. Büdel, Remote Sens. Environ. **112**, 2187 (2008).